A three-band perfect absorber based on a parallelogram metamaterial slab with monolayer MoS_2

Wen-Jing Zhang(张雯婧)[1,2], Qing-Song Liu(刘青松)[1,2], Bo Cheng(程波)[1,2], Ming-Hao Chao(晁明豪)[1,2], Yun Xu(徐云)[1,2], and Guo-Feng Song(宋国峰)[1,2,†]

[1] *Institute of Semiconductors, Chinese Academy of Sciences, Beijing* 100083, *China*

[2] *College of Materials Science and Opto-Electronic Technology, University of Chinese Academy of Sciences, Beijing* 100049, *China*

(Received 21 June 2022; revised manuscript received 21 August 2022; accepted manuscript online 8 September 2022)

As a two-dimensional (2D) material, monolayer MoS_2 which limits its optical applications has a low absorption efficiency. In this paper, we propose a three-band perfect metamaterial absorber in the visible light range based on monolayer MoS_2. The peak absorptivity of the structure at each resonance wavelength is nearly perfect, moreover, the light absorption of monolayer MoS_2 is obviously enhanced at the three resonant wavelengths. The dielectric–dielectric–metal structure we designed produces the coupling of Fabry–Perot resonance and high-order diffraction guided-mode resonance at different absorption peaks, which has been proved by the slab waveguide theory. In addition, the multi-modal absorption phenomenon is explained by extracting the equivalent impedance. The results show that we can adjust the absorption peak wavelength by regulating the parameters of the structure. This structure not only provides an idea for enhancing the interaction between light and two-dimensional materials but also has potential applications for optical detection devices.

Keywords: metamaterial, perfect absorber, monolayer MoS_2, high-order diffraction

PACS: 42.79.Gn, 81.05.Xj, 02.70.Bf **DOI:** 10.1088/1674-1056/ac9047

1. Introduction

Metamaterials mean artificial composite structures or composite materials with unusual electromagnetic properties, made up of artificially microstructures. Different electromagnetic properties can be achieved by designing different microstructures, resulting in different propagation modes of electromagnetic waves.[1,2] Metamaterials bring entirely new optical properties, such as negative refractive index. The rise of metamaterials provides a way to realize many applications. Metamaterials have sub-wavelength scales volume, making it easier to integrate ultra-compact optical devices than that of three-dimensional bulk materials.[3] In 2008, Landy *et al.* achieved the first metamaterial absorber with an absorptivity close to 100%.[4] Over the few years, metamaterial perfect absorbers (MPA) have attracted a lot of interest from researchers and have been proved useful in practical applications, such as sensors,[5] filters,[6] energy harvestings[7] and photodetectors.[8]

In recent years, the rise of graphene[9–11] has triggered much research on two-dimensional (2D) materials and their related structures. This kind of material with atomic thickness has unique optical properties, which has aroused great discussion in the field of optoelectronics.[12–14] MoS_2 is one of the representative materials of transition metal disulfides (TMDCs), which will transform from indirect band gap to direct band gap semiconductor with the decrease of layers,[15–17] and this feature makes it has a great application prospect in photoluminescence[18] and photodetectors.[19] Because the inherent thickness of the atomic layers, the absorptivity of monolayer MoS_2 in the visible light range is very low, about only 10%,[20] which greatly limits the use of monolayer MoS_2. Up to now, much work has been done to enhance the absorption of monolayer MoS_2, and several methods have been reported. Li *et al.* achieved perfect light absorption of monolayer MoS_2 in both theoretically and numerically through the method of critical coupling with guided resonances.[21] Lu *et al.* used a novel multilayer photonic structure, because of the excitation of the Tamm plasmon mode, the absorptivity reached 96%.[22] In addition, the magnetically coupled metasurface of Ag nanograting/space layer/Ag reflector structure is also proved to be an effective structure to enhance the absorption of monolayer MoS_2.[23] However, there are not many reports about selective absorbers based on the MoS_2, which can be used in frequency-selective photodetectors and sensors. However, the multiband perfect absorbers have great applications in multispectral detection and sensors.

In this paper, we propose a three-band and tunable selective metamaterial absorber in the visible region, which consists of a periodic stereoscopic dielectric parallelogram, a dielectric layer, an Al substrate, and a monolayer MoS_2 sandwiched in the dielectric layer. The finite-difference time-domain (FDTD) simulations demonstrate that nearly perfect absorption in the three prominent display peaks, and the spectral positions of absorption peaks can be tuned by changing the structural parameters. When the impedance of the structure matches the impedance of free space, the reflectivity is almost zero ac-

†Corresponding author. E-mail: sgf@semi.ac.cn

© 2023 Chinese Physical Society and IOP Publishing Ltd

cording to the impedance matching theory.[4] The results show that the proposed structure can excite high-order diffraction guided-mode resonance and FP resonance, thus achieving efficient absorption. This structure provides a new idea for enhancing the interaction between monolayer MoS_2 and light and achieving selective absorption, it also has important applications in MoS_2 photodetector and photoluminescence.

2. Structure and model

As shown in Fig. 1, our proposed absorber consists of monolayer MoS_2, dielectric material and metal silver substrate. The top layer is composed of two axisymmetric solid parallelograms and the material is TiO_2, followed by HfO_2 dielectric layer and Al metal backplane. A monolayer MoS_2 is sandwiched in the dielectric layer. The refractive index of TiO_2 and HfO_2 are set as 2.36[24] and 1.975,[25] respectively. The material properties of Al are adopted from the Palik's optical constants handbook.[26] In the simulation, the thickness of monolayer MoS_2 was set as $d = 0.65$ nm. In order to save the simulation time, we chose monolayer MoS_2 as the 2D conductivity model and the permittivity of MoS_2 was measured by Beal *et al.*[27] The sizes of the axisymmetric parallelogram are $L_1 = 150$ nm, $L_2 = 240$ nm, $L_3 = 130$ nm, and $H_1 = 70$ nm and the periods are $P_x = 580$ nm and $P_y = 240$ nm, respectively. The thicknesses of the dielectric layer are $H_2 = 120$ nm and $H_3 = 430$ nm, respectively. The thickness of Al substrate is $H_4 = 150$ nm so that all incident light is reflected back, and the transmittance is basically 0. Then the absorption of the structure can be expressed as $A = 1 - R$ (R is the reflectivity of the proposed structure). The structure can be fabricated by the atomic layer deposition (ALD) method to grow HfO_2 and electron beam lithography (EBL) to prepare surface patterns.[28]

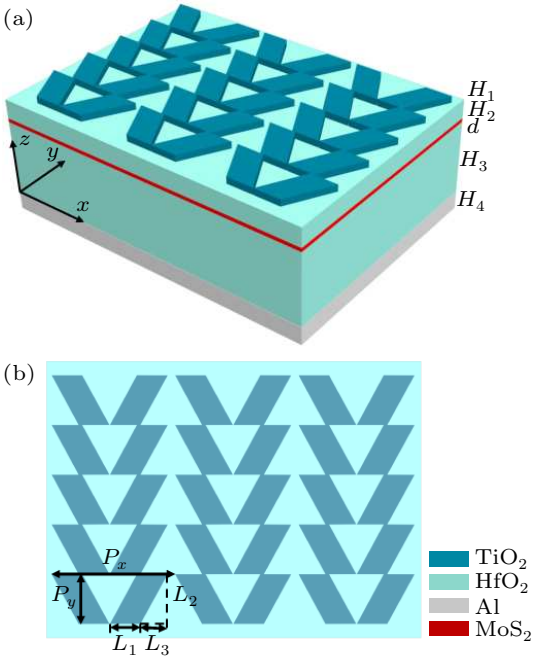


Fig. 1. (a) Schematic diagram of the proposed structure illuminated by normal incident TE wave; (b) the top view of the structure. The parameters are $L_1 = 150$ nm, $L_2 = 240$ nm, $L_3 = 130$ nm, $P_x = 580$ nm, $P_y = 240$ nm.

In this paper, we use Lumerical FDTD solutions for numerical calculations. The TE polarization (the electrical field polarized along x axis) plane wave is used to illuminate the structure, and the accuracy of mesh in FDTD is set to 4. Periodic boundary conditions are set in x and y directions, and perfect matched layer boundary conditions are set in z direction, and then a single cell is simulated.

3. Results and discussion

Figure 2(a) shows the absorption spectrum of the structure, at 454 nm, 502 nm, and 551 nm, the absorptivity reached 99%, 96%, and 99%, respectively. In order to calculate the light absorption of monolayer MoS_2, we refer to[29]

$$A(\lambda) = \frac{4\pi c}{\lambda}\mathrm{Re}(N)\cdot\mathrm{Im}(N)\cdot\int_{V_1}|E_1|^2\,\mathrm{d}V_1, \tag{1}$$

which is expressed by the ration of electromagnetic energy absorbed by monolayer MoS_2 to incident electromagnetic energy. In Eq. (1), c is the speed of light in vacuum, N is the refractive index of monolayer MoS_2,[27] E_1 and V_1 are the local electric field and the volume in the monolayer MoS_2, respectively, λ is the wavelength of incident light. By integrating the electric field inside of the MoS_2 and calculating, we obtain the absorptivity of monolayer MoS_2. From the absorption spectrum of monolayer MoS_2, we can observe that the absorptivity of monolayer MoS_2 at the three resonance wavelengths reaches 52%, 22%, and 19%, respectively. This shows that our proposed structure can also enhance the absorption of monolayer MoS_2.

We calculate the impedance of the structure to explain the physical mechanism of the three peaks. According to the impedance matching theory, when the impedance of the structure is close to that of the free space, a very small reflection is produced.[4,30] In the calculation of impedance (Z), the S parameters and the impedance Z can be expressed as

$$S_{11} = S_{22} = \frac{\mathrm{i}}{2}\left(\frac{1}{Z} - Z\right)\sin(nkH), \tag{2}$$

$$S_{12} = S_{21} = \frac{1}{\cos(nkH) - \frac{\mathrm{i}}{2}\left(\frac{1}{Z} + \frac{1}{2}\right)\sin(nkH)}, \tag{3}$$

$$Z = \pm\sqrt{\frac{(1+S_{11})^2 - S_{21}^2}{(1-S_{11})^2 - S_{21}^2}}, \tag{4}$$

where S_{11}, S_{12}, S_{22}, S_{21} are S parameters, n is the effective refractive index of the structure, k is the electromagnetic wave vector, and $H = H_1 + H_2 + H_3 + d$. The impedance of the free space is $Z_0 = \sqrt{\frac{\mu(\omega)}{\varepsilon(\omega)}} = 1$. It can be observed from Fig. 2(b) that at the three resonance wavelengths, the real part of the

impedance is close to 1 and the imaginary part is close to 0, which content the impedance matching condition.

From Fig. 2(a), we can observe that the high absorptivity mainly comes from the resonance of the structure. In the following, we study the physical mechanism of the absorber through the distribution of electric fields. We take the cross-sectional electric field 60 nm away from the upper edge of the parallelogram in y-direction. From Fig. 3, we can observe that the electric field is mainly concentrated in the cavity and a small part is confined to the edge of the surface structure and the interface between the metal and the dielectric layer. The electric field of the surface structure has a positive effect on the absorptivity. Moreover, there is a standing wave excitation in the z-direction of the dielectric layer, which proves that the main resonance is formed in the cavity, which is the characteristic of guided-mode resonance.[31] In addition, the electric field at each wavelength contains local electric fields of different intensity, we can speculate that there is more than one resonance mode of the structure.

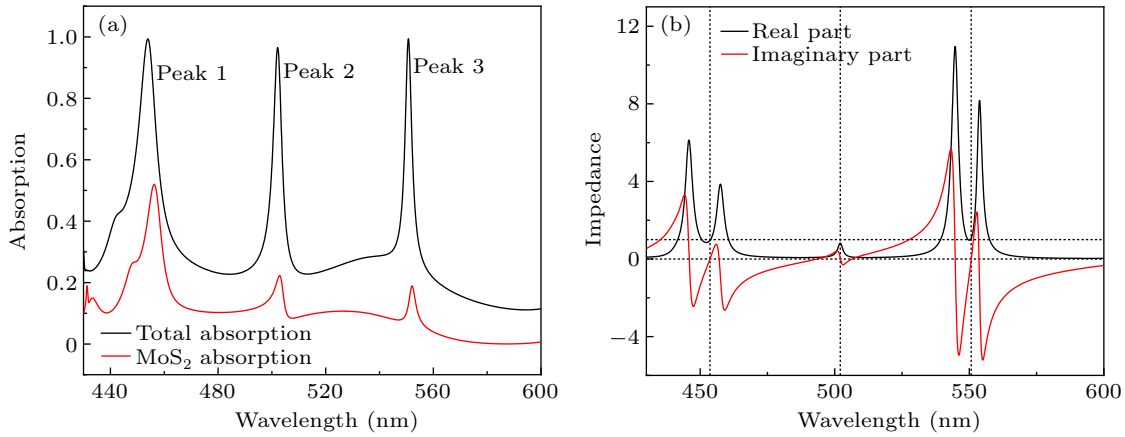


Fig. 2. (a) Absorptance spectrum of the proposed structure. (b) Real (black line) and imaginary (red line) parts of the input impedance of the structure.

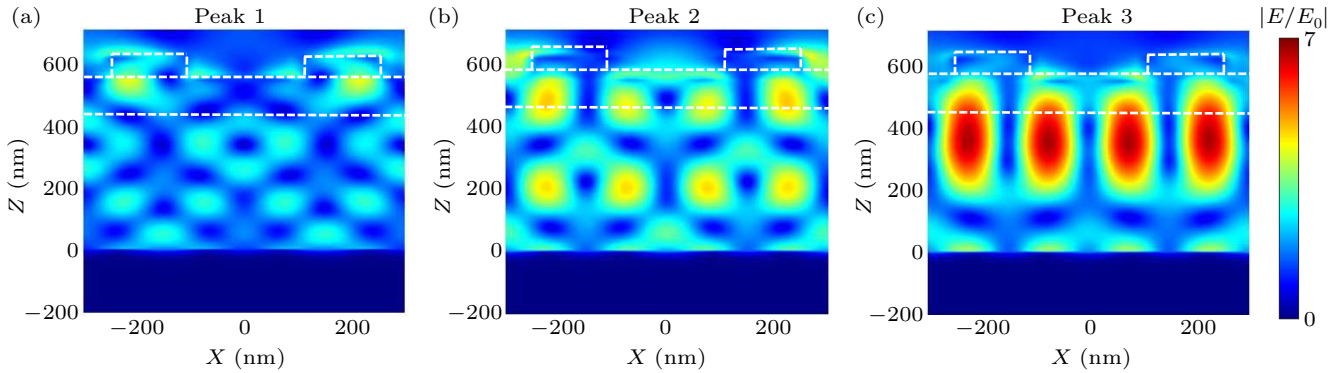


Fig. 3. Electric field distributions in the x–z plane at (a) 454 nm; (b) 502 nm; (c) 551 nm, and the white lines represent the interfaces between materials in the structure.

In order to further research the origin of the resonance of the structure, we use the rigorous coupled-wave analysis (RCWA) to calculate the absorption of the structure of the first-order diffraction without the monolayer MoS_2. We calculate the variation trend of resonance wavelength of the first-order diffraction with dielectric layer thickness H_3, as shown in Fig. 4(a). This hybrid structure can be broadly considered as a Fabry–Perot (F–P) cavity resonator. After the wave is reflected several times by the reflection surface in the cavity, there will has the effect of constructive interference, which leads to the reinforcement of the wave. When the propagating phase in the dielectric layer increases by integer multiples of 2π and the increase in the thickness of the dielectric layer by $\lambda_s/2$ ($\lambda_s = \lambda/n_s$ being the wavelength inside of the spacer medium), the conditions of constructive interference are still satisfied therefore higher-order cavity modes will be generated.[32,33] The resonance wavelength of the first-order diffraction satisfies the phase matching condition[34]

$$2nh = \left(q - \frac{\varphi}{2\pi}\right)\lambda, \tag{5}$$

where n is the refractive index of the FP cavity, h is the thickness of the dielectric layer, φ is the total shift of the upper and lower interfaces of the FP cavity, q is an integer, λ is the resonance wavelength of the FP cavity. We calculate the variation trend of resonance wavelength with the thickness of the dielectric layer through Eq. (5), as shown in Fig. 4(b). As can be seen from Fig. 4, the positions of the calculated formant are basically consistent with those calculated by RCWA, which proves

that the resonance of the first-order diffraction of the structure designed by us comes from FP resonance. It can be concluded that the three main resonance peaks in Fig. 2(a) are generated by the high-order diffraction of the incident light.[35]

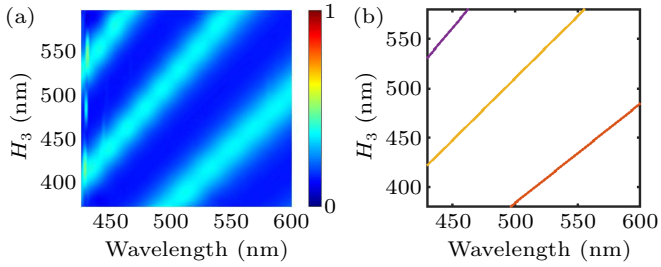


Fig. 4. Spectra of the structure of the first-order diffraction without the monolayer MoS_2. (a) Absorption calculated by RCWA. (b) Resonance wavelength calculated by Eq. (5).

Next, we calculate the variation trend of the absorption containing high-order diffraction with the change of the thickness of the dielectric layer H_3 through FDTD, as shown in Fig. 5(a). At the same time, we estimate the variation of resonance wavelengths associated with waveguide layer thickness H_3 in TE mode by slab waveguide theory.[36–38] The effective propagation constant of the mode is

$$\beta_i = k\left(n_1 \sin\theta - i\frac{\lambda}{P}\right), \tag{6}$$

where $k = 2\pi/\lambda$, λ is the wavelength in the free space, n_1 is the refractive index of the incident dielectric, θ is the incident angle, i is the diffraction order, and P is the period of the structure.

According to the effective media theory (EMT), the top TiO_2 layer can be replaced by a plane plate with a certain refractive index in the calculation, and the effective refractive index n_2 of TiO_2 layer can be approximated as

$$n_2 = \sqrt{(1-f)n_{\mathrm{g}}^2 + f n_{\mathrm{r}}^2}, \tag{7}$$

where n_{g} and n_{r} are the refractive index of the grating groove and grating ridge, respectively, f is the grating filling factor. Thus, we can obtain the intrinsic equation of the four-layer waveguide by using the known refractive of the four layers of materials.

The wavenumbers of the cover layer (here is air), the TiO_2 pattern layer, the HfO_2 layer, and the substrate can be expressed as

$$p_1 = \left(\beta^2 - k_0^2 n_1^2\right)^{1/2}, \tag{8}$$

$$k_2 = \left(k_0^2 n_2^2 - \beta^2\right)^{1/2}, \tag{9}$$

$$k_3 = \left(k_0^2 n_3^2 - \beta^2\right)^{1/2}, \tag{10}$$

$$p_4 = \left(\beta^2 - k_0^2 n_4^2\right)^{1/2}. \tag{11}$$

The eigenvalue equation of the four-layer waveguide is

$$k_3 d_{\mathrm{w}} = m\pi + \arctan\left(\frac{p_1}{k_2}\right) + \arctan\left(\frac{p_2}{k_3}\right), \tag{12}$$

where $p_2 = k_2 \tan[\arctan(p_1/k_2) - k_2 d_{\mathrm{g}}]$, β is the propagation constant of the waveguide, m is the order of waveguide mode. To excite the guided-mode resonance in the structure, the incident light must satisfy the wave vector matching condition

$$\beta = \beta_i, \tag{13}$$

where i is the diffraction order.

Thus, we estimate the resonant wavelength using the dispersion relation of the slab waveguide. Figure 5(b) shows the relationship between cavity thickness H_3 and resonance wavelength. From Fig. 5(b), we can get the resonance wavelength of different orders guided-mode resonance at the second-order diffraction. The resonance peaks estimated by using the dispersion relation of slab waveguide are nearly consistent with the calculated result of FDTD. Therefore, we can get that the resonance of the structure comes from the second-order diffraction guided-mode resonance. When the resonance conditions of the first-order diffraction resonance and the second-order diffraction resonance are reached simultaneously, the two modes will intersect, and high absorption occurs. If they have an odd π-phase difference, destructive interference will occur, the energy can not be effectively located, forming the breakpoints in Fig. 5(a).

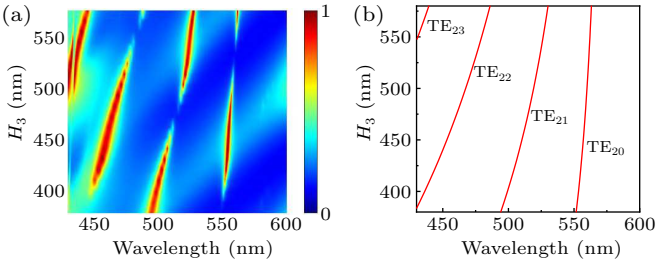


Fig. 5. Absorption property (a) calculated by FDTD; (b) estimated by the slab waveguide theory. And other parameters are set as default.

In order to investigate the effects of structure parameters on absorptivity, we change some sizes of the structure for analysis. As can be seen in Fig. 6(a), all three peaks will change regularly with the change of period. As the P_x increases from 560 nm to 600 nm, the location of peak 1 moves from 444 nm to 464 nm, the location of peak 2 moves from 491 nm to 516 nm, and the location of peak 3 moves from 534 nm to 569 nm. With the increase of the period, the resonance wavelengths of the three absorption peaks of the structure all show a red-shift phenomenon. The change of period also leads to the change of absorptivity, but most of the peak absorptions remain above 90%. The change of structure parameters will not cause the change of absorptivity if it is a single resonance mode. However, in our proposed structure, there has resonance coupling at two diffraction orders, so the absorptivity will change as the period changes. We also study the effect

of P_y on the absorption spectrum. When P_y increases, a weak blue shift occurs in the absorption spectrum, and the absorptivity of peak 2 and peak 3 decreases significantly. The change of period not only affects the coupling between modes, but also affects the effective refractive index of the pattern layer, which leads to the change of the resonance and absorptivity. For parallelogram blocks, if L_3 and P_x increase at the same time and the others remain unchanged, the shape of two symmetrical parallelograms will also change. As shown in Fig. 6(c), when L_3 increases from 120 nm to 150 nm, the location of the three absorption peaks will also have a very significant red-shift phenomenon. By changing the L_3 parameters of the parallelogram, the displacement of the three absorption peaks covers almost the whole band of 450 nm to 600 nm. The reason for the phenomenon is that the three absorption peaks are induced by cavity mode, the increase of L_3 will increase the effective refractive index of the upper interface of the cavity, so the peaks experience a red-shift.

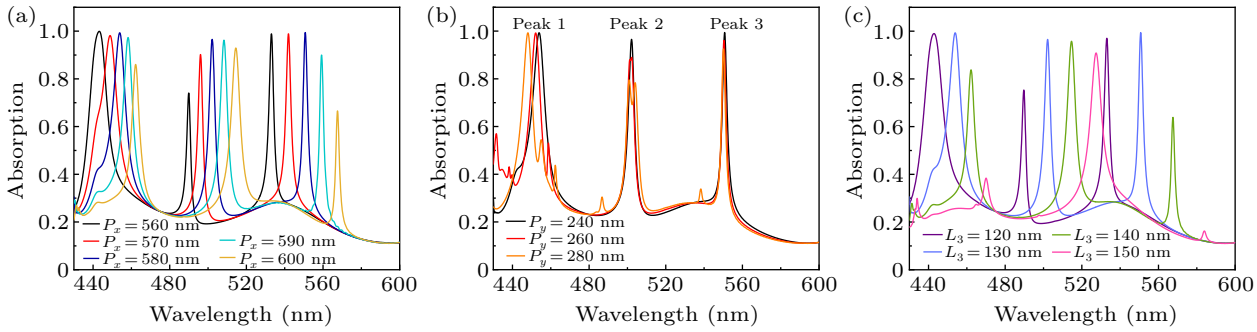


Fig. 6. Absorption spectra of the structure analysis with varying (a) P_x, (b) P_y, and (c) L_3, respectively. And other parameters are set as default.

We further investigate the influence of the incident light on the spectral absorptance of the structure. When the polarization angles change by 90°, the polarization direction changes from TE to TM. We can observe from Fig. 7(a) that when the polarization angle is increased gradually from 0° to 45°, the location changes of the three peaks are not great, but the absorptivity will change a lot. With the further increase of polarization angle, the resonance wavelength of the absorption peaks will change. The resonance wavelengths are different when TE and TM polarized lights are the incident light, but a high absorptivity can be maintained respectively. The resonance wavelengths caused by TE and TM incident light are different, which is caused by the mode splitting between TE and TM.[39] When the polarization angle is not 0° or 90°, the incident light can be decomposed into two vectors of TE mode and TM mode, and the absorptivity is the superposition of the absorption caused by the light with different energy in two polarized directions. Therefore, when the polarization angle changes, the absorptivity of TE and TM modes will also change respectively. Since our microstructure is an axially symmetric pattern with no chiral response, there is no difference between the absorption of left-circularly polarized and right-circularly polarized light incident.

Figure 7(b) shows the absorption spectra with different incident angles. We can observe that when the incident angle varies from 0° to 10°, there still appears a strong resonance absorption phenomenon. However, each absorption peak splits into two bands, the two peaks after splitting appear red-shift and blue-shift respectively with the increase of the incident angle. Since the absorption peak mainly comes from the cavity mode, when the incident angle is not 0°, the spatial symmetry of the diffracted wave in the cavity will be destroyed, no effective interference can be formed, so absorption peaks exhibit frequency splitting phenomenon.[40,41] At the same time, when the incident light at some angles, the resonance absorption phenomenon becomes weakens or disappears. This proves that in these cases, there is no strong resonance or effective standing wave in the cavity. Therefore, we can flexibly adjust the position and intensity of the absorption peak in the spectrum by regulating the incident light angle.

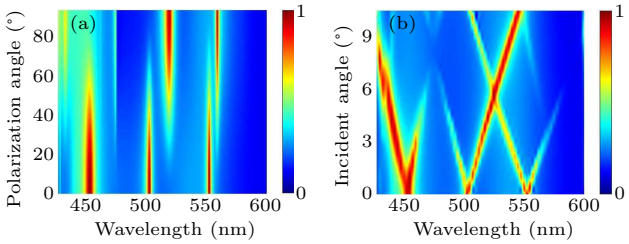


Fig. 7. Absorption spectra of the structure versus (a) polarization angle of incident light; (b) incident angle.

4. Conclusion and perspectives

In conclusion, we propose a three-band perfect absorber in the visible light range based on a dielectric–dielectric–metal structure. At three resonance wavelengths, the structure not only achieves nearly perfect light absorption but also effectively enhances the interaction between light and monolayer MoS_2. The high light absorptions of the structure are caused by the coupling of high-order diffraction guided-mode resonance and FP resonance, and this structure is effective in enhancing the light absorption of other 2D materials, not lim-

ited to MoS_2. The calculation of impedance shows that the real and imaginary parts at absorption wavelength satisfy the impedance matching theory. In addition, the influence of the geometrical parameters of the structure on the spectral absorption is investigated, and it is proved that the absorption spectral nearly coverages from 450 nm to 600 nm can be achieved by adjusting the geometric parameters. The proposed structure can be applied to narrow-band selective sensors, thermal emitters, optical detection devices and has potential applications in spectral imaging.

Acknowledgments

Project supported by the Strategic Priority Research Program of Chinese Academy of Sciences (Grant No. XDB43010000), the National Natural Science Foundation of China (Grant Nos. 61835011 and 12075244), Key Research Projects of the Frontier Science of the Chinese Academy of Sciences (Grant No. QYZDY-SSW-JSC004), and the National Key Research and Development Program of China (Grant No. 2020YFB2206103).

The authors would like to thank Dr. Jie-Tao Liu for his help in calculation and language editing.

References

[1] Shalaev V M 2007 *Nat. Photon.* **1** 41
[2] Zheludev N I and Kivshar Y S 2012 *Nat. Mater.* **11** 917
[3] Liu Q S, Cheng B, Chao M H, Zhang W J, Xu Y and Song G F 2021 *Ann. Phys.* **533** 2100255
[4] Landy N I, Sajuyigbe S, Mock J J, Smith D R and Padilla W J 2008 *Phys. Rev. Lett.* **100** 207402
[5] Bakir M, Karaaslan M, Unal E, Akgol O and Sabah C 2017 *Opto-Electron. Rev.* **25** 318
[6] Gao Y X, Ren G B, Zhu B F, Huang L, Li H S, Yin B and Jian S S 2016 *Plasmonics* **11** 291
[7] Ghaderi B, Nayyeri V, Soleimani M and Ramahi O M 2018 *Sci. Rep.* **8** 13227
[8] Rosenberg J, Shenoi R V, Vandervelde T E, Krishna S and Painter O 2009 *Appl. Phys. Lett.* **95** 161101
[9] Geim A K and Novoselov K S 2007 *Nat. Mater.* **6** 183
[10] Xia S X, Zhai X, Huang Y, Liu J Q, Wang L L and Wen S C 2017 *Opt. Lett.* **42** 3052
[11] Guan J R, Xia S X, Zhang Z Y, Wu J, Meng H Y, Yue J, Zhai X, Wang L L and Wen S C 2020 *Nanoscale Res. Lett.* **15** 142
[12] Geim A K and Grigorieva I V 2013 *Nature* **499** 419
[13] Koppens F H L, Mueller T, Avouris P, Ferrari A C, Vitiello M S and Polini M 2014 *Nat. Nanotechnol.* **9** 780
[14] Xu M S, Liang T, Shi M M and Chen H Z 2013 *Chem. Rev.* **113** 3766
[15] Zhang Y, Zhang X Z, Deng C Y, Ge Q, Huang J J, Lu J, Lin G X, Weng Z K, Zhang X A and Cai W W 2020 *Chin. Phys. B* **29** 067403
[16] Mak K F and Shan J 2016 *Nat. Photon.* **10** 216
[17] Wang Q H, Kalantar-Zadeh K, Kis A, Coleman J N and Strano M S 2012 *Nat. Nanotechnol.* **7** 699
[18] Splendiani A, Sun L, Zhang Y B, Li T S, Kim J, Chim C Y, Galli G and Wang F 2010 *Nano Lett.* **10** 1271
[19] Lopez-Sanchez O, Lembke D, Kayci M, Radenovic A and Kis A 2013 *Nat. Nanotechnol.* **8** 497
[20] Bernardi M, Palummo M and Grossman J C 2013 *Nano Lett.* **13** 3664
[21] Li H J, Qin M, Wang L L, Zhai X, Ren R Z and Hu J G 2017 *Opt. Express* **25** 31612
[22] Lu H, Gan X T, Mao D, Fan Y C, Yang D X and Zhao J L 2017 *Opt. Express* **25** 21630
[23] Long Y B, Deng H D, Xu H T, Shen L, Guo W B, Liu C Y, Huang W H, Peng W T, Li L X, Lin H J and Guo C 2017 *Opt. Mater. Express* **7** 100
[24] Siefke T, Kroker S, Pfeiffer K, Puffky O, Dietrich K, Franta D, Ohlidal I, Szeghalmi A, Kley E B and Tunnermann A 2016 *Adv. Opt. Mater.* **4** 1780
[25] Priambodo P S, Maldonado T A and Magnusson R 2003 *Appl. Phys. Lett.* **83** 3248
[26] Palik E D 1997 *Handbook of Optical Constants of Solids* (Burlington: Academic Press) pp. xvii–xviii
[27] Hsu C W, Frisenda R, Schmidt R, Arora A, de Vasconcellos S M, Bratschitsch R, van der Zant H S J and Castellanos-Gomez A 2019 *Adv. Opt. Mater.* **7** 1900239
[28] Qing Y M, Ma H F, Yu S and Cui T J 2019 *J. Appl. Phys.* **125** 213108
[29] Jackson J D 2003 *Classical Electrodynamics* (New York: Wiley) p. 1
[30] Mei P, Zhang S, Lin X Q and Pedersen G F 2019 *IEEE Antennas Wirel. Propag. Lett.* **18** 521
[31] Wu J, Liu X Y and Huang Z 2021 *Chin. Phys. B* **30** 014202
[32] Bhattarai K, Silva S, Song K, Urbas A, Lee S J, Ku Z and Zhou J F 2017 *Sci. Rep.* **7** 10569
[33] Qiu C Y, Wu J H, Zhu R R, Shen L and Zheng B 2019 *Opt. Commun.* **451** 226
[34] Massiot I, Colin C, Sauvan C, Lalanne P, Cabarrocas P R I, Pelouard J L and Collin S 2013 *Opt. Express* **21** A372
[35] Nie J Q, Yu J C, Liu W X, Yu T B and Gao P Q 2020 *Opt. Express* **28** 38592
[36] Wang J P, Jin Y X, Ma J Y, Shao J D and Fan Z X 2010 *Chin. Phys. B* **19** 054202
[37] Sang T, Yin X, Qi H L, Gao J, Niu X S and Jiao H F 2020 *IEEE Photon. J.* **12** 4500111
[38] Wang S S and Magnusson R 1995 *Appl. Optics* **34** 2414
[39] Kaliteevski M, Iorsh I, Brand S, Abram R A, Chamberlain J M, Kavokin A V and Shelykh I A 2007 *Phys. Rev. B* **76** 165415
[40] You S P, He Y, Yang Y F and Zhang H F 2017 *Chin. Phys. B* **26** 030301
[41] Piper J R and Fan S 2014 *ACS Photon.* **1** 347